Heterogeneous interface induced electrocatalytic efficiency boosting of bimetallic Cu/Zn selenides for stable water oxidation and oxygen reduction reactions

Muthuraja Velpandian[a], Govind Ummethala[b], Sairam K Malladi[b], Praveen Meduri [a*]

[a] Department of Chemical Engineering, Indian Institute of Technology Hyderabad, Kandi, Sangareddy-502285, Telangana (India)

[b] Department of Materials Science and Metallurgical Engineering, Indian Institute of Technology Hyderabad, Kandi, Sangareddy-502285, Telangana (India)

Table S1 Fitted values of R_s, R_{ct} and C_{dl} with the circuit shown in Fig. S7.

Sample	R_s, Ω	R_{ct}, Ω	C_{dl}, μF
CZSe@C-450	29.04	16.3	6.59
CZSe@C-550	29.12	24.6	10.1
CZSe@C-350	29.95	27.3	16.7
CuSe@C	31	28.28	17.2
ZnSe@C	30.02	28.31	19.3

Determination of electrochemical surface area:

The electrochemical surface area (ECSA) is determined using double layer capacitance. CVs are acquired by varying the scan rate (0.1 V s⁻¹ to 0.8 V s⁻¹; Fig. S8) wherein, current is measured where both anodic and cathodic scans are parallel to one another (non-faradaic potential region) at a particular potential and plotted against the corresponding scan rate which follows the following equation:

$$I_c = v\, C_{dl}$$

where I_c is the double layer charging current, v is the scan rate and C_{dl} is the double layer capacitance associated with it, which is the slope of the linear plot between I_c vs v.

ECSA of an electrocatalyst is then calculated using the following equation:

$$ECSA = \frac{C_{dl}}{C_S}$$

where the specific capacitance C_S is of the atomically smooth planar surface of the same material under similar experimental conditions. The reported value of C_S is 0.04 mF cm⁻² in alkaline conditions and is used to calculate ECSA in this study[1].

Table S2 Calculated values of ECSA.

Sample	ECSA, cm²
CZSe@C-450	4.70
CZSe@C-550	2.74
CZSe@C-350	2.35
CuSe@C	0.12
ZnSe@C	0.11

Determination of Turnover frequency (TOF):

TOF is calculated using the following equation[2]:

$$TOF = \frac{J}{4 \, F \, N_s}$$

where J, F and N_s are current density at a certain overpotential (A cm^{-2}), Faraday constant (96485 C mol^{-1}) and concentration of active sites in the catalyst (mol cm^{-2}), respectively.

N_s is determined using the following relation[2]:

$$\frac{i_{peak}}{v} = \frac{n^2 F^2 A \, N_s}{4 \, RT}$$

where $\frac{i_{peak}}{v}$, n, R, and T are the slope of the plot generated between peak current and scan rate using CV's at different scan rates in the potential range of the reaction (Fig. S9), number of electrons transferred, ideal gas constant and absolute temperature, respectively.

Table S3 Calculated values of N_s (concentration of active sites) and TOF (turn over frequency).

Sample	N_s, mol cm^{-2}	TOF, s^{-1} (at current density of 10 mA cm^{-2})
CZSe@C-450	1.16E-7	0.22
CZSe@C-550	1.34E-7	0.19
CZSe@C-350	3.12E-7	0.08

Determination of Faradaic efficiency using rotating ring-disk electrode (RRDE):

Rotating ring-disk electrode (RRDE) consists of a Pt ring and a GC disc. CZSe@C-450 is drop-casted on to GC and dried under ambient conditions. LSV (Fig. S11) is generated at a scan rate of 2 mV s^{-1} at 1600 rpm by sweeping the potential from 1.1 to 1.85 V vs. RHE where O_2 is generated (GC disc) and the generated O_2 is reduced at the Pt ring where a constant potential of −0.5 V is applied to enable an efficient oxygen reduction reaction (ORR). Faradaic efficiency is calculated using the following equation[3]:

$$Faradaic\ Efficiency\ = \frac{I_R\ n_D}{I_D\ n_R\ N_{CL}}$$

where I_R is the ring current due to the reduction of oxygen, I_D is the disk current due to the evolution of oxygen, n_D and n_R are the numbers of electrons transferred during the evolution and reduction of O_2 (both are 4). The parameter N_{CL} indicates the collection efficiency of RRDE, which can be determined using a ferrocyanide/ferricyanide redox couple. An average N_{CL} of 0.3684 is used which is in fair agreement with that of a commercially provided RRDE comprising of a GC disc and a Pt ring (0.37).

Determination of number of electrons in ORR:

The number of electrons transferred (n) is obtained by Koutecky-Levich (K-L) equation as follows[4]:

$$\frac{1}{j} = \frac{1}{B\sqrt{\omega}} + \frac{1}{j_k}$$

$$B = 0.62 \, n \, F \, D^{\frac{2}{3}} \, \gamma^{\frac{-1}{6}} \, C$$

where j is the current density, j_k is the kinetic current density, ω is the electrode rotation rate, n is the electron transfer number, F is the Faraday constant ($F = 96485$ C mol^{-1}), C is the concentration of dissolved O_2 in 0.1M KOH ($C_o = 1.2 \times 10^{-6}$ mol cm^{-3}), D is the diffusion coefficient of O_2 in 0.1M KOH ($D = 1.9 \times 10^{-5}$ cm^2 s^{-1}), γ is the kinematic viscosity of 0.1M KOH ($\gamma = 0.01$ cm^2 s^{-1}).

Table S4 Kinetic parameters of CZSe@C-450 for ORR at different potentials.

Potential, V	Slope	Intercept	No. of electrons	j_k, mA cm^{-2}
0.7	2.75	0.26	3.27	-3.80
0.6	2.75	0.16	3.26	-6.14
0.55	2.85	0.14	3.15	-6.92
0.5	2.96	0.13	3.03	-7.55
0.45	2.98	0.11	3.02	-8.51
0.4	2.89	0.11	3.10	-8.60
0.35	2.71	0.11	3.31	-8.37
0.3	2.52	0.15	3.56	-6.43

RRDE experiment is used to verify the electron transfer number (n) during ORR using the equation below:

$$n = \frac{4\,|I_D|}{|I_D| + \dfrac{I_R}{N}}$$

The hydrogen peroxide production yield is calculated by the equation below:

$$\%H_2O_2\ yield = \frac{200 * \dfrac{i_R}{N}}{|i_D| + \dfrac{i_R}{N}}$$

where I_R is the ring current, I_D is the disk current and N indicates the collection efficiency of RRDE which can be determined using a ferrocyanide/ferricyanide redox couple. An average N value of 0.3684 is used which is in fair agreement with that of a commercially provided RRDE comprising of a GC disc and a Pt ring (0.37).

Determination of mass activity and specific activity of ORR electrocatalysis:

The mass activity is calculated using the kinetic current at 0.8 V vs RHE in the ORR polarisation curve normalized by the catalyst loading. The specific activity is calculated using the kinetic current at 0.8 V vs RHE normalized by the Brunauer− Emmett−Teller (BET) surface area.

Table S5 Comparison of electrochemical performance of copper and zinc based electrocatalysts.
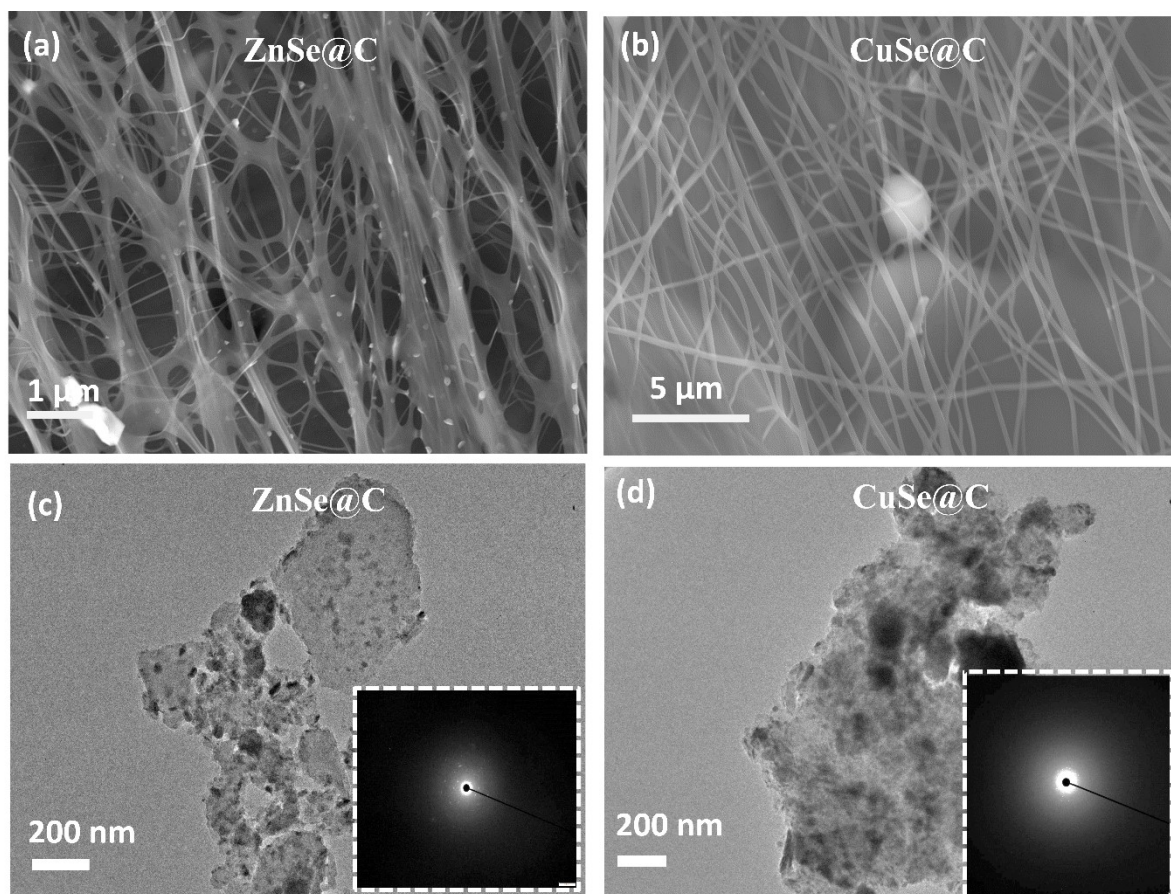
Electrocatalyst	Synthesis Method	Electrolyte	Over potential (mV vs RHE)	Tafel Slope (mV/dec)	Reference
Electrocatalytic Oxygen Evolution Reaction					
CZSe@C-450	Electrospinning & selenisation	1 M NaOH	260	62	This work
Cu_2Se	Electrodeposition	1M KOH	270	107.6	5
Cu_2Se	Hydrothermal	1M KOH	290	136.7	5
Cu_2Se	CVD	1M KOH	300	90.9	5
Cu_2Se	Electrodeposition	1M KOH	320	48.1	5
CuSe/NF	Solid state	1M KOH	297	89	6
$Cu(OH)_2$ NWS/CF	Simple chemical reaction and oxidation	0.1 M NaOH	530	86	7
CuO NWS	Simple chemical reaction and oxidation	0.1 M NaOH	590	84	7
CuOx NWS	Simple chemical reaction and oxidation	0.1 M NaOH	630	108	7
Annealed CuO	Electrodeposition	1 M KOH	430(1 mA cm^{-2})	61.4	8
H_2O_2 treated CuO	Hydrothermal	0.1 M KOH	520(2.5mA cm^{-2})	-	9
$Cu_{0.3}Ir_{0.7}O_\delta$	Hydrothermal	1 M KOH	415	105	10
$CuCo_2O_4$−SSM	Sacrificial support method	1 M KOH	420	-	11
$CuRhO_2$	Coprecipitation	0.1 M KOH	400	81	12
Cu_3P/CF	Surface oxidation	1 M KOH	412 (50mA cm^{-2})	63	13
Cu_3P/ CuO core shell nanorod arrays	Electrochemical oxidation	1M KOH	315	74.8	14
Cu2S/CF nanosheet		1M KOH	336 (20 mA cm^{-2})	101	15
CuO/C nano dendritic	Electrodeposition	1 M NaOH	290	67.5	16
CuCo2S4 nanosheets	Hydrothermal	1M KOH	310	86	17

CuO nanowire	Electrodeposition	1M Na_2CO_3	580	86	18
Cu/Cu(OH)2-CuO nanorods	anodisation	0.1 M KOH	417	76	19
Cu_2Se core/shell nanotube arrays	Simple chemical reaction immersion	1 M KOH	200	150	20
Cu_2Se-Cu_2O film	Electrodeposition	0.2M carbonate buffer	465	140	21
Cu_2S branch arrays	Electrodeposition and sulfurization	1M KOH	284	72	22
Ce modified CuO_x	Electrodeposition	0.1 M KOH	400	74	23
CuO nanowire	Wet chemistry annealing	1M Na_2CO_3	500	41	24
$CuCo_2Se_4$ @ Au	Hydrothermal	1M KOH	320	66.5	25
Fe-doped MOF CuCoSe@HCNFs	Hydrothermal & sacrificial agent annealing	1M KOH	260 (20mA cm^{-2})	57	26
Cu_2Se/$NiSe_2$/NF	Hydrothermal	1 M KOH	277 (50mA cm^{-2})	40.17	27
ZnSe with reduced titania	Solvothermal	0.1 M KOH	570	45	28

Electrocatalytic Oxygen Reduction Reaction

Electrocatalyst	Synthesis Method	Electrolyte	J_L (mA cm^{-2})	$E_{1/2}$ (V)	Reference
CZSe@C-450	Electrospinning & selenisation	0.1M KOH	3.65	0.88 V vs RHE	This work
Cu_{2-x} Se	Chemical synthesis	0.1M KOH	4	-0.21 V vs Ag/Agcl	29
CuSe decorated CNT	Hydrothermal	0.1M KOH	2.37	0.5 V vs Ag/Agcl	30
CuSe @ graphene CNT	Hydrothermal	0.1M KOH	4.5	-0.12 V vs SCE	31
N doped Graphene/ZnSe	Hydrothermal	1M KOH	2.4	-1.85 V vs Hg/HgO	32
Co0.62Zn0.38Se@NCF-800	Electrospinning & pyrolysis	0.1M KOH	5.05	0.83 Vs RHE	33

Cu precursor
Zn precursor
+Se

DMF

V

Electrospinning

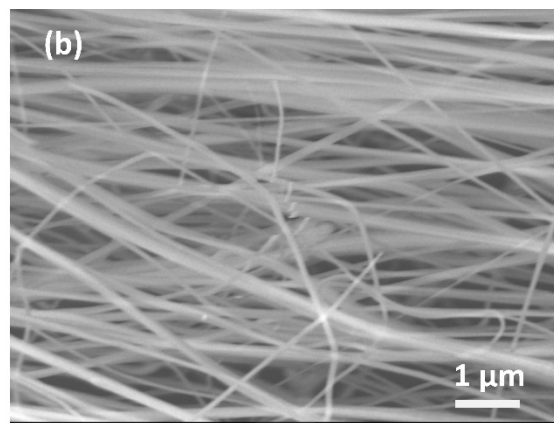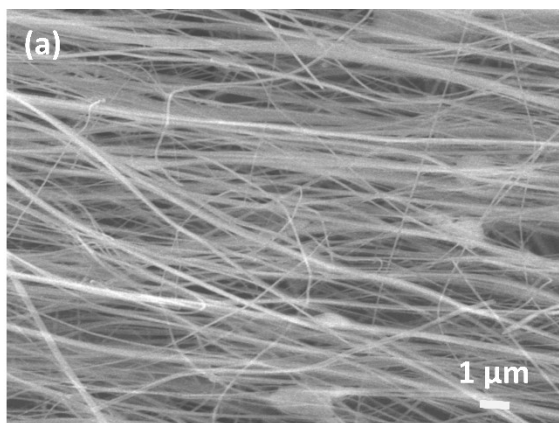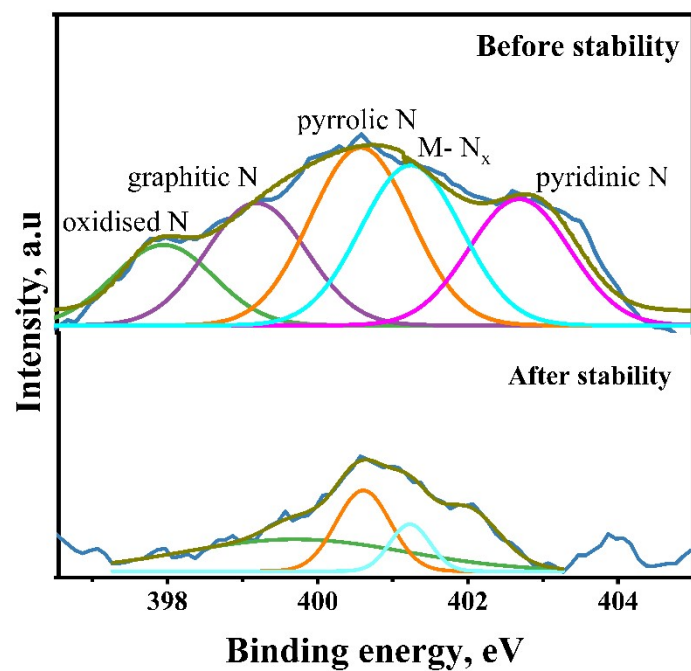High temperature Annealing

CZSe@C nanofibres

Fig
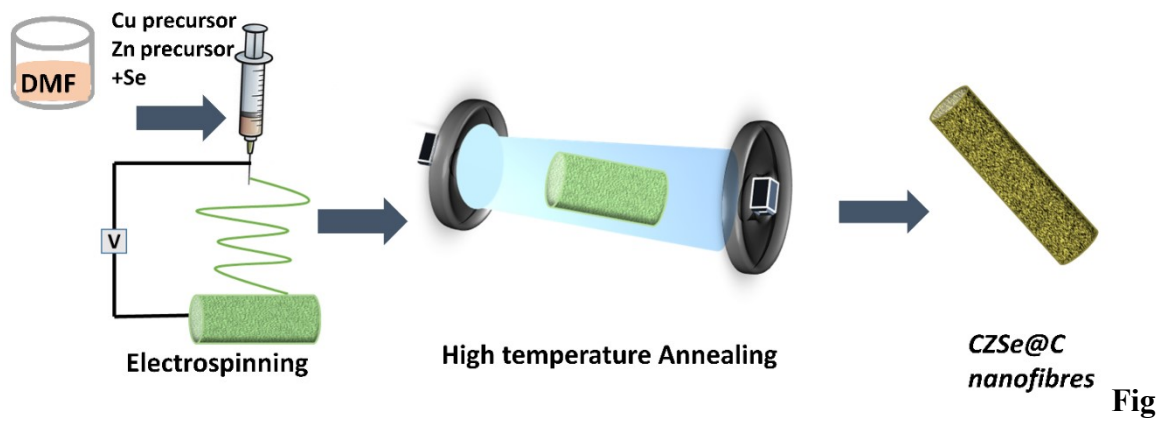
. S1 Schematic representation of electrode fabrication via electrospinning.
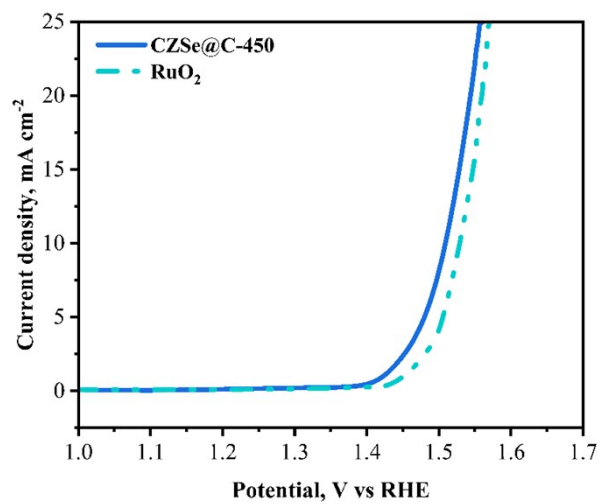
Fig. S2 SEM images: (a) ZnSe@C. (b) CuSe@C. TEM images of: (c) ZnSe@C at low resolution with an inset of SAED. (d) CuSe@C at low resolution with an inset of SAED.
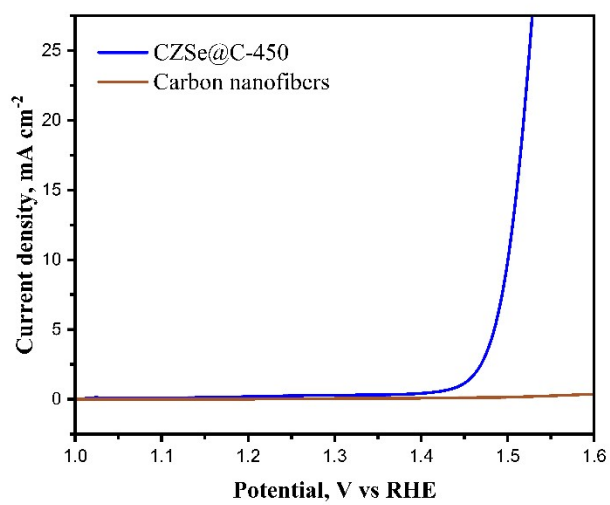
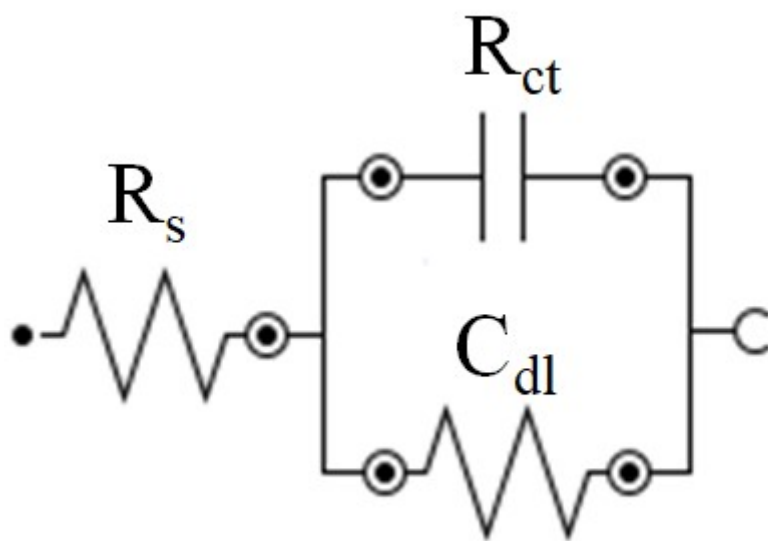**Fig. S3** SEM images: (a) & (b) CZSe@C nanofibers before annealing.

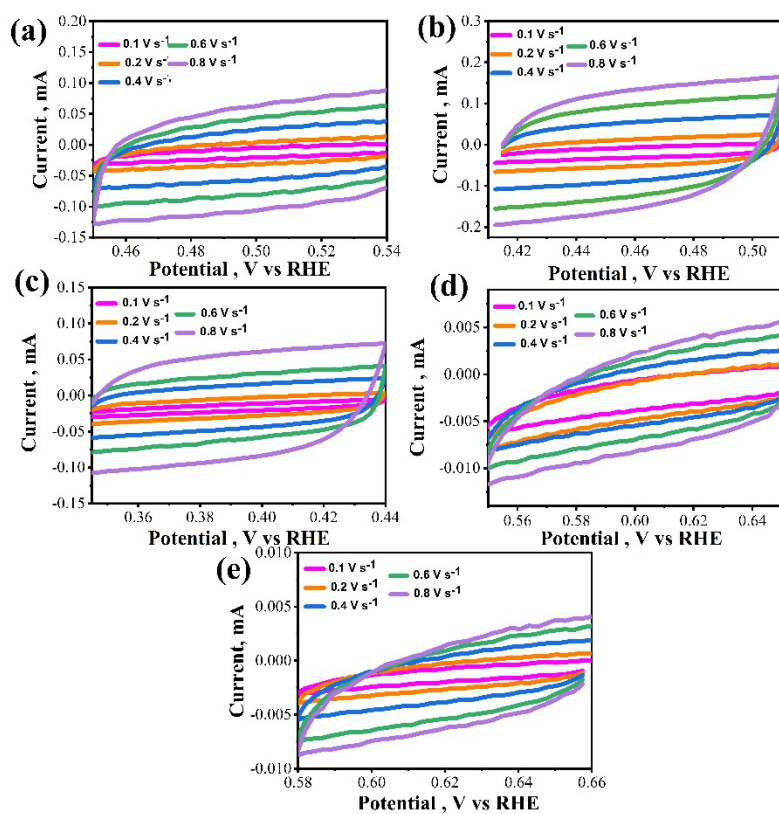**Fig. S4** XPS N 1s spectra of CZSe@C-450 (before and after stability).

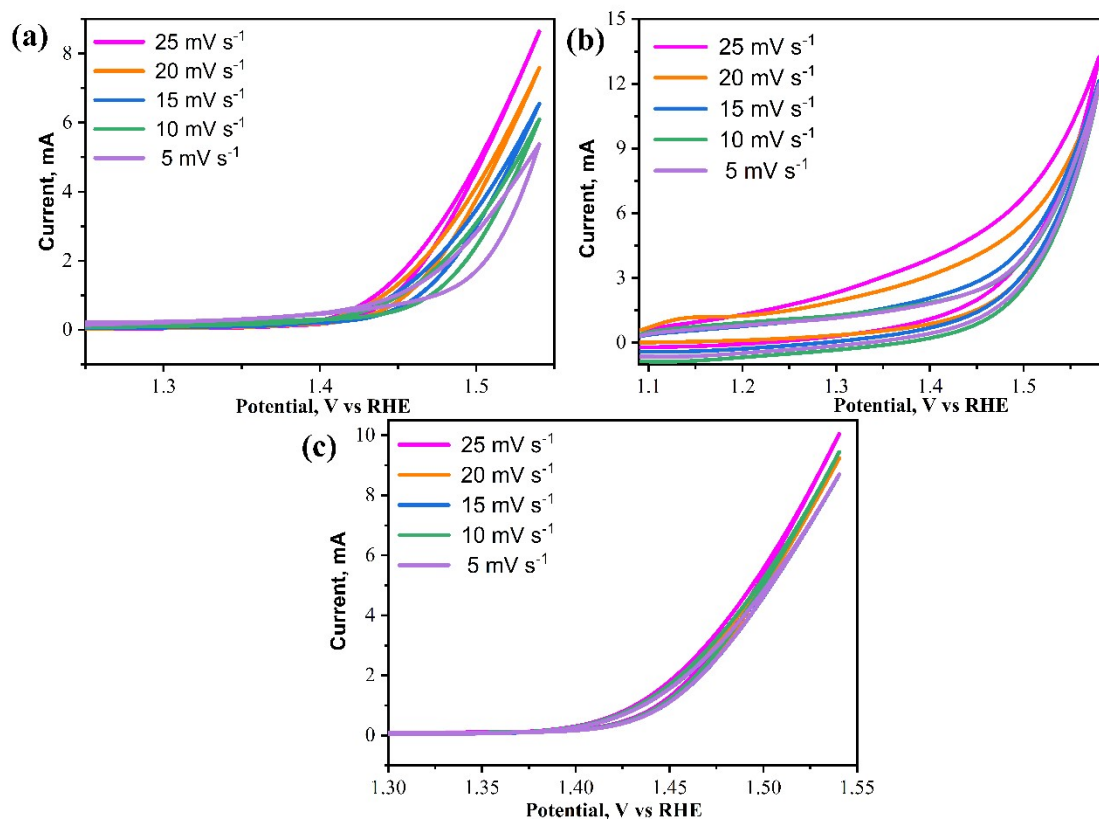**Fig. S5** LSV curve of CZSe@C-450 and RuO$_2$.

Fig. S6 LSV (OER) of CZSe@C-450 and carbon nanofibers.

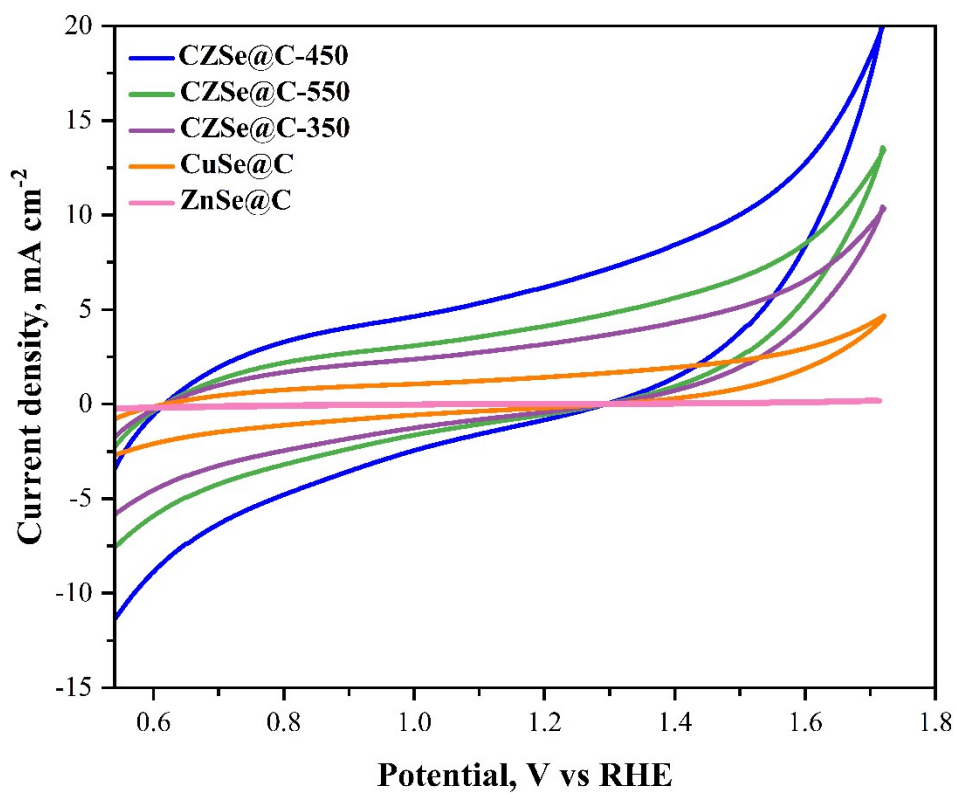**Fig. S7** Equivalent circuit fit of EIS data.

Fig. S8 Cyclic voltammetry curves (non-faradaic region) at various scan rates: (a) CZSe@C-350. (b) CZSe@C-450. (c) CZSe@C-550. (d) CuSe@C. (e) ZnSe@C.
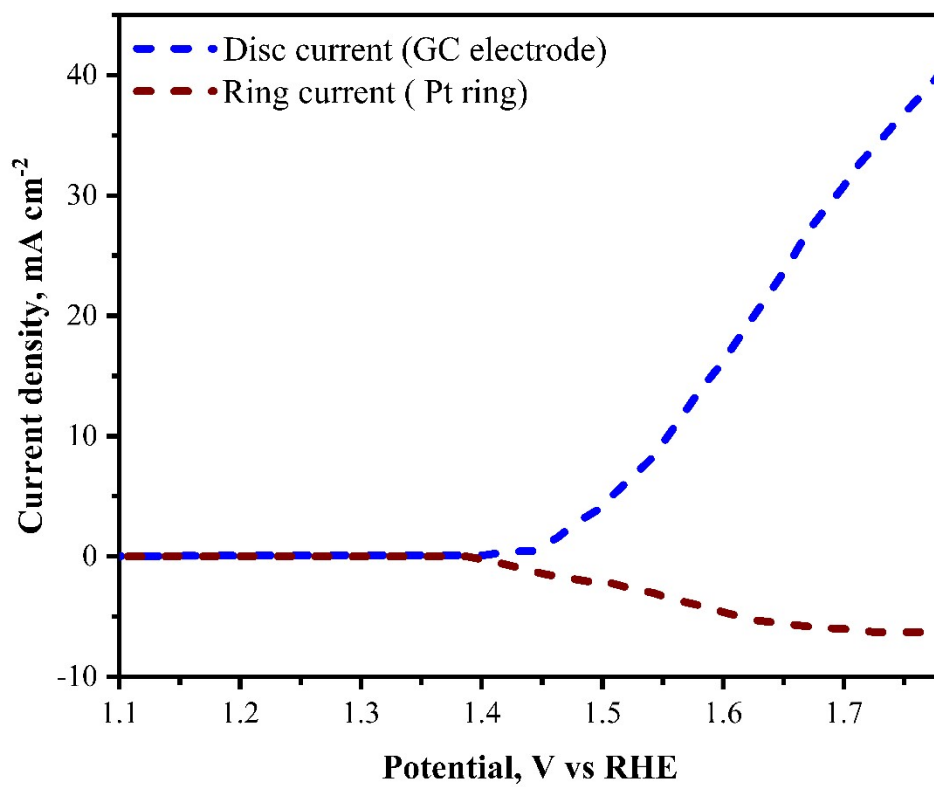
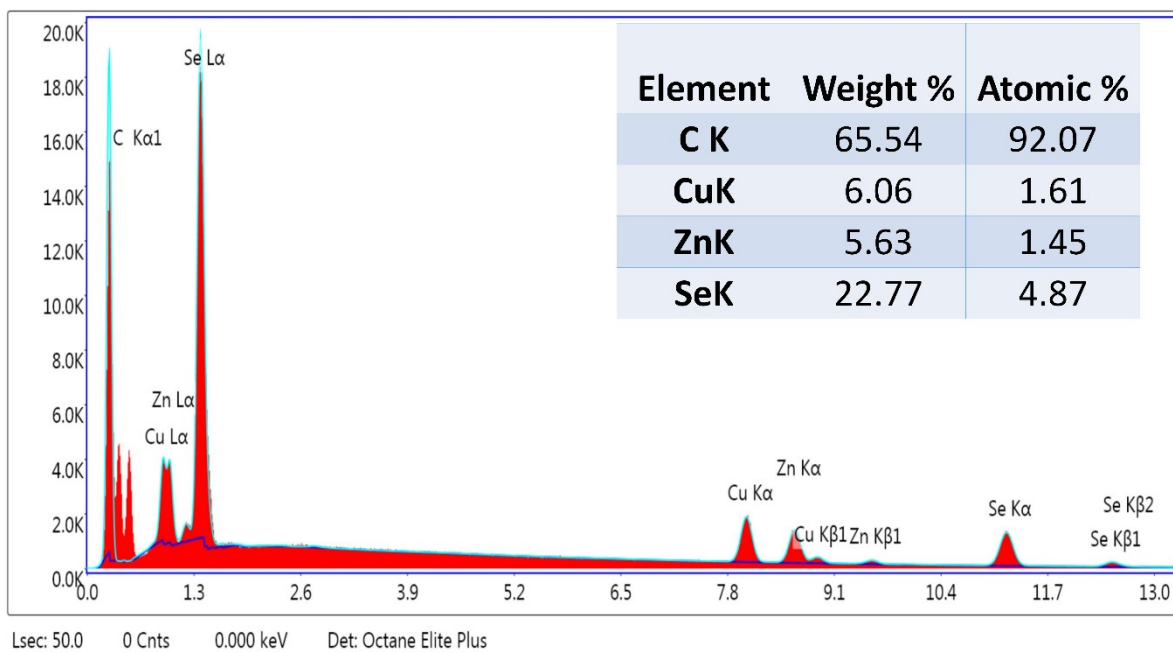**Fig. S9** Cyclic voltammetry curves at various scan rates: (a) CZSe@C-350. (b) CZSe@C-450. (c) CZSe@C-550.

Fig. S10 Cyclic voltammetry curves of CuSe@C, ZnSe@C, CZSe@C-350, CZSe@C-450, and CZSe@C-550.

Fig. S11 Ring current and disc current of RRDE linear sweep voltammetry for CZSe@C-450.

Element	Weight %	Atomic %
C K	65.54	92.07
CuK	6.06	1.61
ZnK	5.63	1.45
SeK	22.77	4.87

Lsec: 50.0   0 Cnts   0.000 keV   Det: Octane Elite Plus

Fig. S12 EDX analysis of CZSe@C-450 before testing.
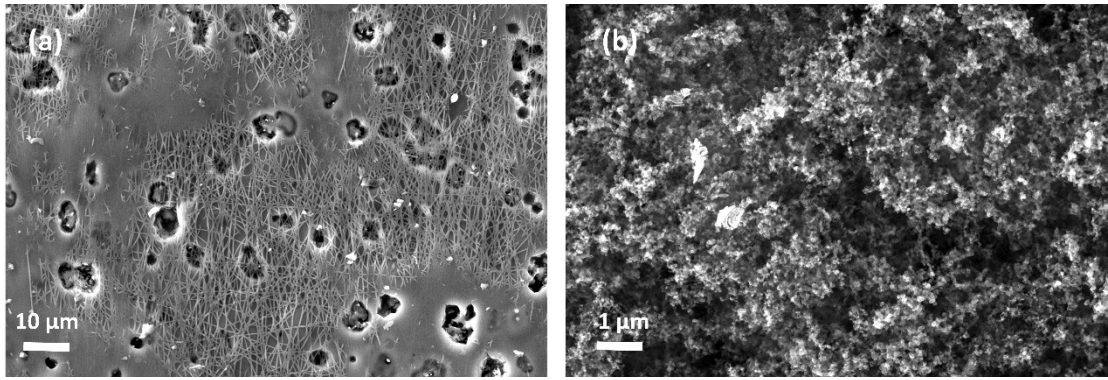
Fig. S13 SEM analysis of CZSe@C-450 after stability testing for: a) 12 hours. b) 50 hours.
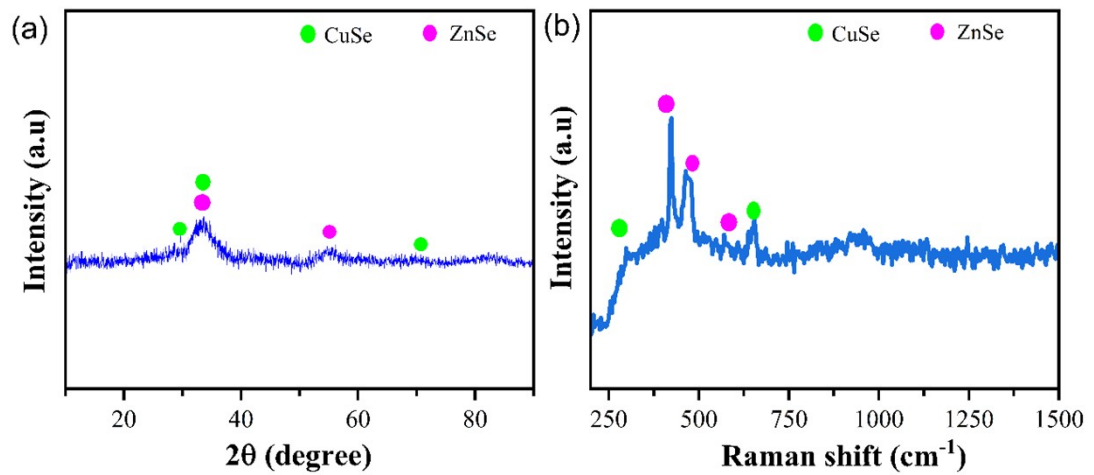
Fig. S14 Post 50-hour stability analysis of CZSe@C-450 using: a) XRD. b) Raman.

Fig. S15 ORR polarisation curve of CZSe@C-450 and Pd/C at 1500 rpm.
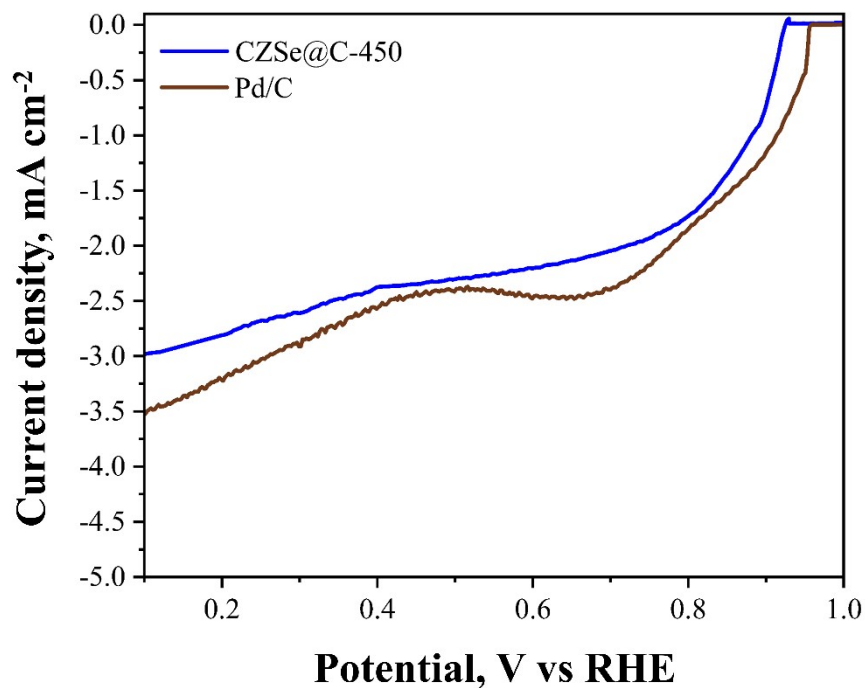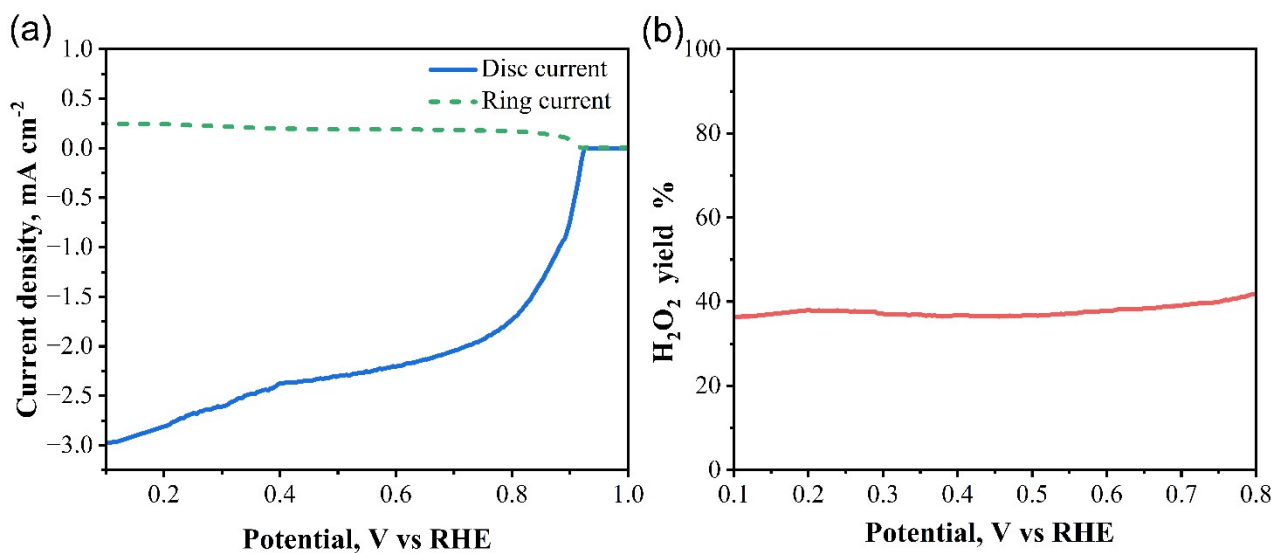

Fig. S16 Rotating ring–disk electrode (RRDE) analysis during ORR of CZSe@C-450

: a) determination of electron transfer number. b) H_2O_2 yield with potential.
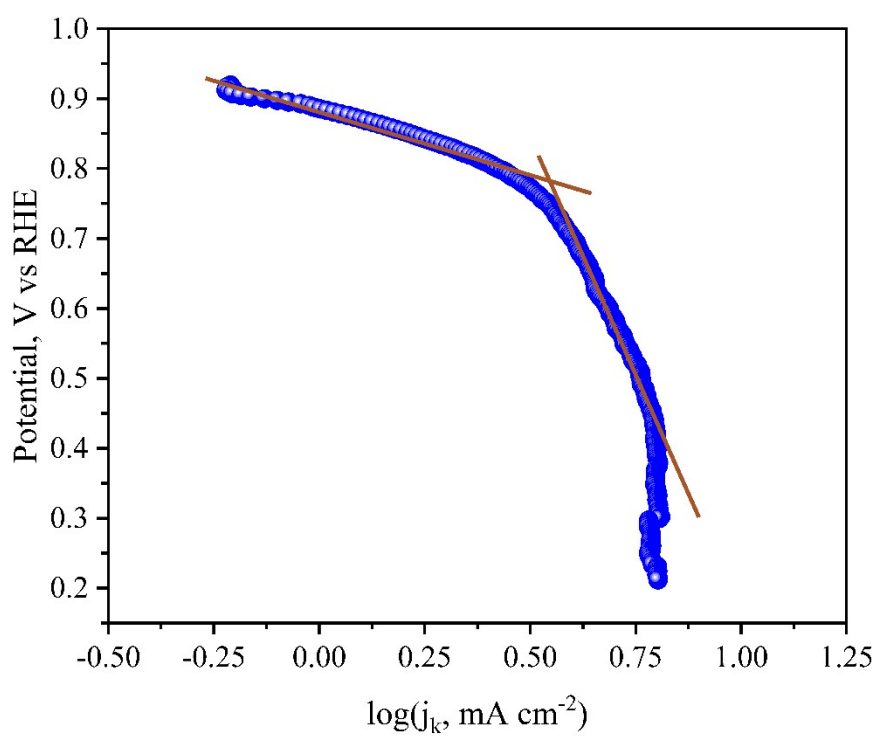
Fig. S17 Mass transfer correlated Tafel plot for ORR of CZSe@C-450.

Table S6 Tafel slope and exchange current density values for ORR of CZSe@C-450.

Region	Tafel slope, mV dec⁻¹	Exchange current density, mA cm⁻²
Higher potential	263	0.83
Lower potential	2878	2.63
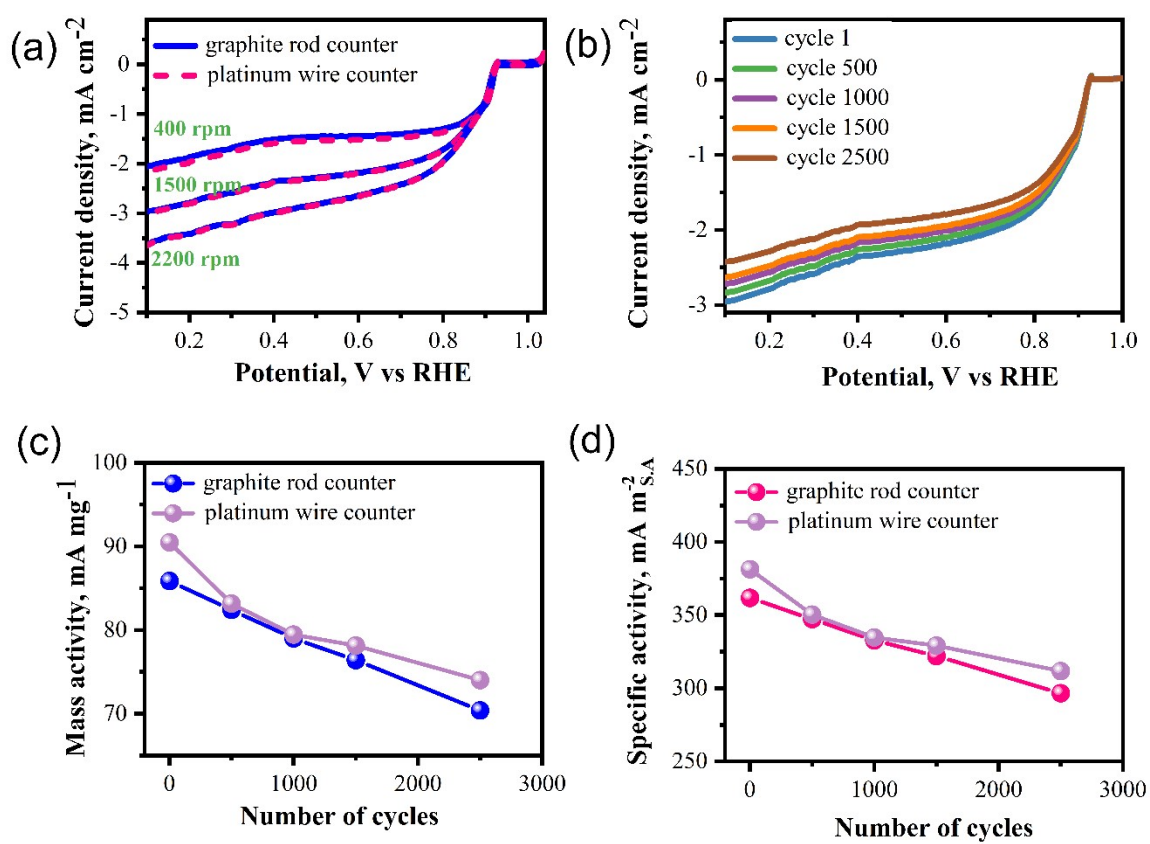
Fig. S18 CZSe@C-450 ORR polarization using graphite rod as counter electrode: a) LSV at different rotating speeds., b) LSV (cycling). c) Mass activity. d) Specific activity.

References:

1. McCrory, C; C. L; Jung, S; Peters, J. C; Jaramillo, T. F. (2013). Benchmarking Heterogeneous Electrocatalysts for the Oxygen Evolution Reaction. Journal of the American Chemical Society, 135(45), 16977–16987. DOI:10.1021/ja407115p

2. Han, H; Choi, H; Mhin, S; Hong, Y.-R; Kim, K. M; Kwon, J; Ali, G; Chung, K; Je, M; Umh,H; Lim, D; Davey, K; Qiao,S; Paik, U; T, Sang. (2019). Advantageous Crystalline-Amorphous Phase Boundary for Enhanced Electrochemical Water Oxidation. Energy & Environmental Science, 12, 2443 2454. DOI:10.1039/c9ee00950g.

3. Anantharaj, S; Ede, S. R; Karthick, K; Sam Sankar, S; Sangeetha, K; Karthik, P. E; & Kundu, S. (2018). Precision and correctness in the evaluation of electrocatalytic water splitting: revisiting activity parameters with a critical assessment. Energy & Environmental Science, 11(4), 744–771. DOI:10.1039/c7ee03457a.

4. Vaughn II, D. D., Araujo, J., Meduri, P., Callejas, J. F., Hickner, M. A., & Schaak, R. E. (2014). Solution Synthesis of Cu_3PdN Nanocrystals as Ternary Metal Nitride Electrocatalysts for the Oxygen Reduction Reaction. Chemistry of Materials, 26(21), 6226–6232. DOI:10.1021/cm5029723.

5. Masud, Jahangir; Liyanage, Wipula P. R.; Cao, Xi; Saxena, Apurv; Nath, Manashi. (2018). Copper Selenides as High-efficiency Electrocatalysts for Oxygen Evolution Reaction. ACS Applied Energy Materials, 1, 4075−4083. DOI:10.1021/acsaem.8b00746.

6. Chakraborty, Biswarup; Beltrán-Suito, Rodrigo; Hlukhyy, Viktor; Schmidt, Johannes; Menezes, Prashanth, W; Driess, Matthias. (2020). Crystalline Copper Selenide as a Reliable Non-Noble Electro(pre)catalyst for Overall Water-Splitting. ChemSusChem, 13(12), 3222–3229. DOI:10.1002/cssc.202000445.

7. Hou, Chun-Chao; Fu, Wen-Fu; Chen, Yong. (2016). Self-Supported Cu-Based Nanowire Arrays as Noble-Metal-Free Electrocatalysts for Oxygen Evolution. ChemSusChem. 9(16), 2069–2073. DOI:10.1002/cssc.201600592.

8. Liu, Xiang; Cui, Shengsheng; Sun, Zijun; Ren, Yang; Zhang, Xiaoyi; Du, Pingwu. (2016). Self-Supported Copper Oxide Electrocatalyst for Water Oxidation at Low Overpotential and Confirmation of Its Robustness by Cu K-Edge X-ray Absorption Spectroscopy. The Journal of Physical Chemistry C. 120, 831−840. DOI: 10.1021/acs.jpcc.5b09818.

9. Handoko, Albertus D; Deng, Suzi; Deng, Yilin; Cheng, Andy Wing Fai; Chan, Kuang Wen; Pan, Yanlin; Tan, Hui Ru; TOK, Eng Soon; Sow, C. H; Yeo, Boon Siang. (2015). Enhanced Activity of H_2O_2 treated Mesostructured Copper (II) Oxide Nanostructures during the Electrochemical Evolution of Oxygen. Catalysis Science & Technology, 6, 269−274. DOI:10.1039/C5CY00861A.

10. Sun, Wei; Song, Ya; Gong, Xue-Qing; Cao, Li-mei; Yang, Ji. (2015). An efficiently tuned d-orbital occupation of IrO_2 by doping with Cu for enhancing the oxygen evolution reaction activity. Chemical science, 6(8), 4993–4999. DOI:10.1039/c5sc01251a.

11. Serov, A.; Andersen, N. I.; Roy, A. J.; Matanovic, I.; Artyushkova, K.; Atanassov, P. (2015). $CuCo_2O_4$ ORR/OER Bi-Functional Catalyst: Influence of Synthetic Approach on Performance. Journal of the Electrochemical Society, 162(4), F449–F454.
DOI: 10.1149/2.0921504jes.

12. Hinogami, R.; Toyoda, K.; Aizawa, M.; Kawasaki, T.; Gyoten, H. (2013). Copper Delafossite Anode for Water Electrolysis. ECS Transactions, 58(2), 27–31.
DOI: 10.1149/05802.0027ecst.

13. Hou, Chun-Chao; Chen, Qian-Qian; Wang, Chuan-Jun; Liang, Fei; Lin, Zheshuai; Fu, Wen-Fu; Chen, Yong. (2016). Self-Supported Cedarlike Semimetallic Cu_3P/CuO Nanoarrays as a 3D High-Performance Janus Electrode for Both Oxygen and Hydrogen Evolution under Basic Conditions. ACS Applied Materials & Interfaces, 8, 23037−23048.
DOI:10.1021/acsami.6b0625.

14. Du, Jian; Li, Fei; Wang, Yong; Zhu, Yong; Sun, Licheng. (2018). Cu_3P/CuO Core-Shell Nanorod Arrays as High-Performance Electrocatalysts for Water Oxidation. ChemElectroChem, 5, 2064−2068.
DOI:10.1002/celc.201800323.

15. He, Liangbo; Zhou, Dan; Lin, Yao; Ge, Ruixiang; Hou, Xiandeng; Sun, Xuping; Zheng, Chengbin. (2018). Ultra-Rapid in Situ Synthesis of Cu_2S Nanosheet Arrays on Copper Foam with Room Temperature Active Iodine Plasma for Efficient and Cost-Effective Oxygen Evolution. ACS Catalysis, 8, 3859−3864.
DOI:10.1021/acscatal.8b00032.

16. Huan, Tran Ngoc; Rousse, Gwenaëlle; Zanna, Sandrine; Lucas, Ivan T.; Xu, Xiangzhen; Menguy, Nicolas; Mougel, Victor; Fontecave, Marc. (2017). A Dendritic Nanostructured Copper Oxide Electrocatalyst for the Oxygen Evolution Reaction. Angewandte Chemie International Edition, 56(17), 4792–4796.
DOI:10.1002/anie.201700388.

17. Chauhan, Meenakshi; Reddy, Kasala Prabhakar; Gopinath, Chinnakonda S.; Deka, Sasanka. (2017). Copper Cobalt Sulphide Nanosheets Realizing Promising Electrocatalytic Oxygen Evolution Reaction. ACS Catalysis, 7, 5871−5879.
DOI:10.1021/acscatal.7b0183.

18. Du, Jialei; Chen, Zuofeng; Ye, Shengrong; Wiley, Benjamin J.; Meyer, Thomas J. (2015). Copper as a Robust and Transparent Electrocatalyst for Water Oxidation. Angewandte Chemie International Edition, 54(7), 2073–2078.
DOI:10.1002/anie.201408854.

19. Cheng, Ningyan; Xue, Yurui; Liu, Qian; Tian, Jingqi; Zhang, Lixue; Asiri, Abdullah M.; Sun, Xuping. (2015). $Cu/(Cu(OH)_2$-CuO) core/shell nanorods array: in-situ growth and application as an efficient 3D oxygen evolution anode. Electrochimica Acta, 163, 102–106.
DOI: 10.1016/j.electacta.2015.02.099.

20. Shi, Wenhui, and Jianshe Lian. (2019). Facile Synthesis of Copper Selenide with Fluffy Intersected-Nanosheets Decorating Nanotubes Structure for Efficient Oxygen Evolution Reaction. International Journal of Hydrogen Energy, 44(41), 22983–90.
DOI: 10.1016/j.ijhydene.2019.07.008.

21. Chen, Hu; Gao, Yan; Ye, Lu; Yao, Yanan; Chen, Xuyang; Wei, Yu; Sun, Licheng. (2018). A Cu_2Se-Cu_2O Film Electrodeposited on Titanium Foil as a Highly Active and

Stable Electrocatalyst for the Oxygen Evolution Reaction. Chemical Communications, 54 (39), 4979–4982.
DOI:10.1039/C8CC02021C.

22. Deng, Shengjue; Shen, Yanbin; Xie, Dong; Lu, Yangfan; Yu, Xiaolong; Yang, Liang; Wang, Xiuli; Xia, Xinhui; Tu, Jiangping. (2019). Directional construction of Cu_2S branch arrays for advanced oxygen evolution reaction. Journal of Energy Chemistry, 39, 61–67.
DOI: 10.1016/j.jechem.2019.01.014.

23. Chen, Zhu; Kronawitter, Coleman; Yang, Xiaofang; Yeh, Yao-Wen; Yao, N; Koel, Bruce E. (2017). Promoting Effect of Tetravalent Cerium on the Oxygen Evolution Activity of Copper Oxide Catalysts. Physical Chemistry Chemical Physics, 19, 31545–31552.
DOI:10.1039/C7CP05248K.

24. Yu, Jun; Cao, Qi; Feng, Bin; Li, Changli; Liu, Jingyuan; Clark, J. Kenji; Delaunay, Jean-Jacques. (2018). Insights into the efficiency and stability of Cu-based nanowires for electrocatalytic oxygen evolution. Nano Research, 11(8), 4323–4332.
DOI:10.1007/s12274-018-2020-1.

25. Cao, Xi; E. Medvedeva, Julia; Nath, Manashi. (2020). Copper Cobalt Selenide as a High-Efficiency Bifunctional Electrocatalyst for Overall Water Splitting: Combined Experimental and Theoretical Study. ACS Applied Energy Materials, 3, 3092–3103.
DOI:10.1021/acsaem.0c00262

26. Chae, Su-Hyeong; Muthurasu, Alagan; Kim, Taewoo; Kim, Jin Soo; Khil, Myung-Seob; Lee, Minju; Kim, Hyoju; Lee, Jun Youb; Kim, Hak Yong. (2021). Templated Fabrication of Perfectly Aligned Metal-Organic Framework-Supported Iron-Doped Copper-Cobalt Selenide Nanostructure on Hollow Carbon Nanofibers for an Efficient Trifunctional Electrode Material. Applied Catalysis B: Environmental, 293, 120209.
DOI: 10.1016/j.apcatb.2021.120209.

27. Bose, Ranjith; Karuppasamy, K.; Arunkumar, Paulraj; Kumar, Veerasubramani Ganesh; Gayathri, Sampath; Santhoshkumar, P.; Vikraman, Dhanasekaran; Han, Jong Hun; Kim, Hyun-Seok; Alfantazi, Akram. (2021). Self-Supportive Bimetallic Selenide Heteronanostructures as High-Efficiency Electro(Pre)Catalysts for Water Oxidation. ACS Sustainable Chemistry & Engineering, 9(38) 13114–23.
DOI:10.1021/acssuschemeng.1c05728.

28. Sadaf, Jamil; Jabeen, Naila; Khan, Latif U.; Bashir, Amna; Janjua, Naveed; Harfouche, Messaoud; Sohail, Manzar. (2021). Synthesis and Comparative Evaluation of Optical and Electrochemical Properties of Efficacious Heterostructured-Nanocatalysts of ZnSe with Commercial and Reduced Titania. Journal of Alloys and Compounds, 879, 160449. DOI: 10.1016/j.jallcom.2021.160449.

29. Yang, Jianping; Chen, Xinqi; Dai, Wei; Wu, Tian; Li, Jie; Luo, Wei; Xu, Kaibing; Xu, Hui; Qin, Feng. (2018). Low-dimensional copper selenide nanostructures: controllable synthesis approach and morphology-dependent electrocatalytic performance. ChemElectroChem, 6 (2), 574–580.
DOI:10.1002/celc.201801130.

30. Tan, Liang; Liu, Zhao-Qing; Li, Nan; Zhang, Jia-Yi; Zhang, Lei; Chen, Shuang. (2016). CuSe decorated carbon nanotubes as a high performance cathode catalyst for

microbial fuel cells. Electrochimica Acta, 213, 283–290. DOI: 10.1016/j.electacta.2016.07.099.

31. Tan, L; Li, N; Chen, S; & Liu, Z.-Q. (2016). Self-assembly synthesis of CuSe@graphene–carbon nanotubes as efficient and robust oxygen reduction electrocatalysts for microbial fuel cells. Journal of Materials Chemistry A, 4(31), 12273–12280. DOI:10.1039/c6ta02891h.

32. Chen, Ping; Xiao, Tian-Yuan; Li, Hui-Hui; Yang, Jing-Jing; Wang, Zheng; Yao, Hong-Bin; Yu, Shu-Hong. (2012). Nitrogen-Doped Graphene/ZnSe Nanocomposites: Hydrothermal Synthesis and Their Enhanced Electrochemical and Photocatalytic Activities. ACS Nano, 6(1), 712–719.
DOI:10.1021/nn204191x.

33. Lv, Li-Ping; Du, Pingping; Liu, Pengbo; Li, Xiaopeng; Wang, Yong. (2020). Integrating Mixed Metallic Selenides/Nitrogen-Doped Carbon Heterostructures in One-Dimensional Carbon Fibers for Efficient Oxygen Reduction Electrocatalysis. ACS Sustainable Chemistry & Engineering, 8(22), 8391–8401.
DOI:10.1021/acssuschemeng.0c02572.